STAFF SUMMARY SHEET

	TO	ACTION	SIGNATURE (Surname), GRADE AND DATE		TO	ACTION	SIGNATURE (Surname), GRADE AND DATE
1	DFAN	sig	Lt Col 27 MAY 14 SHAD A. REED	6			
2	DFER	approve	SOLTZ, AD-22, 27 May 14	7			
3	DFAN	action	(Author /Originator)	8			
4				9			
5				10			

SURNAME OF ACTION OFFICER AND GRADE	SYMBOL	PHONE	TYPIST'S INITIALS	SUSPENSE DATE
McLaughlin, Civ	DFAN	333-2613	tem	20140527

SUBJECT: Clearance for Material for Public Release — USAFA-DF-PA- 341 — DATE: 20140527

SUMMARY

1. PURPOSE. To provide security and policy review on the document at Tab 1 prior to release to the public.

2. BACKGROUND.
Authors: K. Bergeron, Jürgen Seidel, Mehdi Ghoreyshi, Adam Jirasek, Andrew J. Lofthouse, Russell M. Cummings

Title: Numerical Study of Ram Air Airfoils and Upper Surface Bleed-Air Control

Circle one: Abstract Tech Report Journal Article Speech (Paper) (Presentation) Poster
Thesis/Dissertation Book Other: _____

Check all that apply (For Communications Purposes):
[] CRADA (Cooperative Research and Development Agreement) exists
[] Photo/ Video Opportunities [] STEM-outreach Related [] New Invention/ Discovery/ Patent

Description: Natick Soldier Research, Development, and Engineering Center has been leading a Modeling and Simulation effort to develop high fidelity simulations of ram-air parachute systems to complement the design and analysis of new and existing airdrop systems. In this paper an unsteady numerical study of two-dimensional, rigid, ram-air sections with an array of upper surface bleed-air actuators is presented. Aerodynamic forces and lift-to-drag ratios of a modified Clark-Y ram-air airfoil are calculated from unsteady Reynolds-Averaged Navier-Stokes (RANS) simulations, using the Kestrel and Cobalt flow solvers.

Release Information: To be presented at the AIAA AVIATION 2014 Conference, Atlanta, GA, 16-20 June 2014

Previous Clearance information: (If applicable): Released by US Army Natick Research, Development, and Engineering Center

Recommended Distribution Statement: Distribution A: approved for public release, distribution unlimited

3. DISCUSSION.

4. RECOMMENDATION. Sign coord block above indicating document is suitable for public release. Suitability is based solely on the document being unclassified, not jeopardizing DoD interests, and accurately portraying official policy.

Thomas E. McLaughlin, Ph.D.
Director, Aeronautics Research Center

Numerical Study of Ram Air Airfoils and Upper Surface Bleed-Air Control

K. Bergeron*
US Army Natick Research, Development, and Engineering Center, Natick, MA 01760

Jürgen Seidel‡, Mehdi Ghoreyshi†, Adam Jirasek§,
Andrew J. Lofthouse¶, Russell M. Cummings‖
Modeling and Simulation Research Center, U.S. Air Force Academy
USAF Academy, Colorado 80840

Natick Soldier Research, Development, and Engineering Center has been leading a Modeling and Simulation effort to develop high fidelity simulations of ram-air parachute systems to complement the design and analysis of new and existing airdrop systems. In this paper an unsteady numerical study of two-dimensional, rigid, ram-air sections with an array of upper surface bleed-air actuators is presented. Aerodynamic forces and lift-to-drag ratios of a modified Clark-Y ram-air airfoil are calculated from unsteady Reynolds-Averaged Navier-Stokes (RANS) simulations, using the Kestrel and Cobalt flow solvers. The flow fields exhibit a complicated cavity flow coupling with the airfoil profile. Variations in the locations and number of bleed air actuators and trailing edge deflection yield time averaged L/D values between 1.24 and 59.14, and strongly support the utility of the bleed air actuators for use as an enhanced lateral/longitudinal control mechanism. Additionally, these initial results emphasize the requirements for prudent mesh generation and the performance of unsteady calculations for ram-air canopy simulations.

Nomenclature

a	acoustic speed, *m/s*	L/D_{TA}	time averaged lift to drag ratio
b	wing span, *m*	Re	Reynolds Number, Vc/ν
c	airfoil/wind chord, *m*	S	reference area, m^2
c_l	lift coefficient, $L/q_\infty S$	t	time, *s*
c_d	drag coefficient, $D/q_\infty S$	V	velocity, *m/s*
D	drag force, N	x, y, z	grid coordinates, *m*
h	inlet height	α	angle of attack, *rad*
L	lift force	ρ	density, kg/m^3
L/D	lift to drag ratio	ν	air viscosity

I. Introduction

The use of bleed air "spoilers" to increase control authority for personnel airdrop was pioneered and tested for personnel airdrop applications in the mid-1970's by H. Bergeron.[1] J. Hayhurst and J. Eiff also investigated the use of spoilers for personnel use in the mid-1980's[2], and conducted over a hundred test jumps. These personnel systems used a combination of coupled control lines (trailing edge deflection and spoilers) where the bleed air vents opened and closed to spoil the flow across the upper surface of the parachute as depicted in Figure 1. Higgins[3] documents the potential use of a bleed air vent system for autonomously control airdrop systems, and Gavrilovski et al.[4] used a virtual spoiler method on a non-airdrop ram-air gliding

* Senior Research Aerospace Engineer, AIAA Senior Member
† Senior Aerospace Engineer, AIAA Senior Member
‡ Research Associate, AIAA Senior Member
§ Research Fellow, AIAA Senior Member
¶ Director, AIAA Senior Member
‖ Professor of Aeronautics, AIAA Associate Fellow

system for both lateral and longitudinal control. This work was based on wind tunnel testing and preliminary computational fluid dynamics (CFD) work documented in Bergeron et al.[5], and subsequently, led to testing on a 100 ft^2 airdrop system using three independent control motors by Ward and Costello[6] and Bergeron et al.[7]

These last two works showed an enhanced longitudinal control capability which could be coupled to traditional ram-air parachute control inputs thus providing an effective mechanism for increasing the accuracy of guided systems during the terminal phase of the flight. Legacy airdrop systems used differential deflection inputs to produce turn rate response and symmetric inputs to change airspeed, leading to the use of the term "brakes" to identify the control mechanism. Ward[8] has shown the effective use of symmetric brakes for longitudinal control when measured with respect to glide for systems that are oriented into the wind. However, the general use of symmetric brakes results in relatively small changes in L/D as opposed to the use of other longitudinal control devices. While primarily used as a method to enhance longitudinal control, subsequent testing has also proven the effectiveness of using bleed air venting for lateral control. This is accomplished using substantially lower force inputs than trailing edge deflection.

As a result, bleed air vents are being developed for use in Guidance, Navigation, and Control (GN&C) algorithms which will reduce, by an order of magnitude, the power and cost required of autonomously guided airdrop systems. To facilitate this transition, a time-accurate computational simulation capability is being developed to determine steady and dynamic aerodynamic characteristics. Results will serve as the basis for developing control laws for the ram-air parachute bleed air actuators. Ultimately, the results will also be leveraged in conjunction with CFD simulations of appropriate training maneuvers and accurate System IDentification (SID) to develop Reduced Order Models (ROM). Section III below, in particular, addresses flow field characteristics for various bleed air vent configurations as part of the initial phase of control law development. In addition, this report and the work of Ghoreyshi et al.[9] also serve to refine and expand guidelines for future time-accurate simulation studies of ram-air configurations.

A. Two-Dimensional CFD Studies and Lower Surface Separated Flow

Several researchers have presented CFD results for ram-air parachute configurations, and Fogell[10] includes a good overview of these contributions which assume the airfoil surfaces are rigid, impermeable, and smooth. Of particular note for this study is the work of Mittal et al[11], Balaji et al[12], Mohammadi and Johari[13], and Fogell[10], as each of these efforts focused on flow around two-dimensional ram-air airfoil sections. Though the limitations of two-dimensional airfoil simulations, including the inverse energy cascade of turbulent laws (which drives energy into spatially smooth, large eddies—Boffetta and Ecke[14]) and the over-prediction of lift due to the lack of induced drag effects, are well documented, the characterization of ram-air airfoil sections has been useful in determining performance characteristics of new designs. Figure 2 illustrates some of the airfoil sections used in CFD simulations. Though the geometries and definition of airfoil shape parameters have varied, several common observations have been made.

In particular, much attention has been given to a relatively large separation bubble seen downstream of the leading edge to the lower surface. Mittal et al.[11] used a stabilized finite element method (FEM) to find laminar ($Re = 10^4$) and turbulent ($Re = 10^6$ with the Baldwin-Lomax turbulence model) for flows past a Clark-Y airfoil with and without a leading edge cut. The authors note that the flow field over the bottom surface is more severely affected by the

configuration of the cut than the flow field over the upper surface. The authors also report periodic vortex shedding for three configurations of the leading edge cut when conducting turbulent simulations at $Re = 10^6$. Balaji et al.[12] follow a similar line of investigation for an LS(1)-0417 airfoil, and report an $L/D > 25$ for a particular configuration of the leading edge cut at $\alpha = 7.5°$. These two works are particularly noteworthy for their application of CFD to the design process of ram-air canopies. It should also be noted that, as opposed to fixed wing aircraft, ram-air parachute systems are flown in a very narrow range of angles of attack, and the choice of $\alpha = 7.5°$ is a representative configuration for the majority of personnel and cargo airdrop systems.

Mohammed and Johari[13] employ the commercially available finite volume method (FVM) code FLUENT to analyze the flow about a proprietary airfoil shape. Their steady results use the Spalart-Allmaras (SA) turbulence model, and they document lift and drag characteristics at various angles of attack for the baseline and ram-air configurations of the airfoil. They find the difference in the lift-curve slope to only differ from the baseline by 8%. However, they attribute a large influence of cell opening, and associated lower surface separation bubble, on the drag of the ram-air airfoil with an increase of 100% over the baseline for $-4° \leq \alpha \leq 8°$. Again, this study merits recognition for its use of CFD as a design tool.

Fogell[10] pursues a much more ambitious fluid-structure interaction simulation campaign using the commercial flow solver STAR-CCM+ and structural solver LS-DYNA culminating in a 3-D simulation of an infinite span, inflated ram-air configuration. His 2-D CFD simulations follow a geometry definition progression similar to the one followed in Ghoreyshi et al.[9] for validation against the wind tunnel dataset generated by Hiraki and Hidaka.[15] Specifically, Fogell's 2-D simulations characterize the flow field changes of a rounded leading edge, closed inlet, and unstressed cut pattern based on the airfoil section tested by Ware and Hassell[16]. The steady RANS simulations were conducted at $Re = 2.1 \times 10^6$, $\alpha = 5°$, using the Standard and Realizable k-ε turbulence models. While the data aligns with earlier reported results regarding the significant increase in drag due to the open inlet and sharp leading edge, Fogell observes a second contribution to the lower surface separation bubble, in addition to the sharp leading edge. A small portion of the freestream enters the airfoil before being reversed by the stationary pressure field inside the ram-air airfoil. Fogell also reports a significant variation in the flow field, and resulting forces and moments, between the two turbulence models used.

Bergeron et al.[5] used FLUENT to conduct unsteady 2-D CFD simulations, at $Re = 1.6M$ using the SA turbulence model, in support of initial bleed air designs. The baseline geometry represents a slightly thinner airfoil section and lower inlet angle than Fogell, and the different profiles are compared in Figure 2. In particular, Bergeron et al.[5] presented results using an inlet geometry designed to capture certain structural response features, such as "curling," observed from photographs of the airfoil in drop testing. The curled upper surface and lower surface are common aspects of ram-air canopies, and result from balancing the forces and stresses associated with the flow field, suspended weight, material membrane, and support webbing. The simulated flow fields showed significantly less separation on the lower surface than the uncurled baseline airfoil section. The flow field was also observed to enter the airfoil section, as observed by Fogell[10], but it was also less pronounced for the curled than the uncurled inlet geometry. The most notable inlet flow feature associated with this study was the almost complete removal of the reversed flow at the leading edge of the lower surface when then bleed air vent was included in the geometry.

B. Overview

The present work continues the investigation of ram-air flow fields and also addresses the coupling of different configurations of bleed air vents and tail deflection. Results are presented using the FVM solver Kestrel, which has been extensively validated for unsteady CFD for fixed wing aircraft, and the authors suggest computational criteria to follow for unsteady calculations, following the lead of Cummings et al.[17] The results also support parallel work in Ghoreyshi et al.[9] to: 1) propose guidelines for efficient grid generation and 2) reinforce the need for well-defined validation experiments. The paper first reviews the grid generation, flow solver, and computational parameters. Test cases are then described, and results are presented. Finally, conclusions and recommendations are given.

II. Computational Setup

As previously mentioned, this computational effort was conducted in parallel to the results reported in Ghoreyshi et al.[9] Details of the grid convergence study for various geometries as well as a validation results are included in that presentation.

A. Geometry

The baseline geometry used for these simulations is shown in Figure 3, and is based on the cut pattern used in the manufacturing process. Leading edge and vent modifications were made to account for flow-material interactions.[5] Other geometries used within this study have the same leading edge definition and bleed air vent deflection relative to the upper surface profile. All references to the angle of attack, α, are with respect to the horizontal line following the bottom surface of the canopy. This choice is standard practice for parachute manufacturers, and is made for this analysis to facilitate the inclusion of results into future canopy designs.

1. Trailing Edge Deflection

Trailing edge deflections were adapted from the empirical data of Lee and Li.[18] The modeling of deflected trailing edges is a critical component for accurately capturing the dynamic behavior of ram-air parachutes. Standard autonomous guided system control algorithms use a slight trailing edge deflection, approximately 10%, in order to remove the deadband associated with these actuators. 100% deflection is defined approximately when the angle formed by the trailing edge and the lower surface are slightly greater than 90°, and is based on empirical data associated with parachute stall behavior. The precise definition of tail deflection is a nonlinear function of wing loading and canopy material response. Fogell's[10] analyses of fluid membrane interaction confirms the importance of including material modeling distortions and careful implementation of the structural boundary conditions.

The 10% deflection configuration serves as the neutral position for all control inputs, and slightly reduces the *L/D* effectiveness of the airdrop system. However, a more significant constraint to landing accuracy and precision is imposed by this neutral position. During the terminal phases of the guided airdrop system flight path, using a "full-flight" neutral position restricts the system's ability to adapt to strong wind variations which are often encountered. Matos et al.[19] reported an *L/D* variation from 3.1 to 2.1 during wind tunnel testing of a Clark-Y

ram-air canopy, as a function of tail deflection. They also documented a variation in angle of attack, α, between 8.8° for the unrestrained case and 6°, "when maximum flap was applied."

Finally, the deflected tail configuration is used for the "flare," or sink, maneuver necessary for payload survivability during landing. During this portion of the flight, the ram-air canopy is transitioning from a gliding system to a ballistic system.[20] Ward[8] also documents the importance of the longitudinal control authority for symmetric tail deflection. In particular, the effect is strongest for the ground referenced *L/D* as the contribution to drag accounts for accurate and precise landing control.

2. Bleed Air (BA) Vents

Following the process outlined in Bergeron et al.[5], the BA vents for each computational model were set with opening distances of approximately 0.2c and 0.6c depending on the particular geometry tested. The length of the flap was made consistent with previous wind-tunnel models, and the opening distance corresponds to a "small" deflection or, approximately, 25% deflection as measured from the control line. Besides the addition of simulations with BA vents located at 0.6c, an additional parameter was tested—the orientation of the BA vent flap. The flap was either oriented to work as a flow "spoiler" with the flap hinged on the "front" of the vent or as a flow "enhancer" with the flap oriented on the "rear" of the vent. Preliminary drop testing had shown an increase in the system *L/D* for small "rear" openings of a BA vent at the 0.2c location.

B. Computational Grid

Both structured and hybrid grids were tested, but only hybrid results are reported. The hybrid meshes used a refined boundary layer grid along the airfoil surfaces to capture the boundary layer while a tetrahedral grid was used for the circular far field. The far field distance from the middle of the airfoils, which had a chord c = 1m, was 50c. A maximum of 50 layers was chosen with a first cell spacing of 5e-5m. With this spacing, the meshes had a wall $y^+ < 1$ with several mesh layers within the viscous sublayer. In order to maintain quality cell growth and aspect ratio control, cell density with the ram-air airfoils and around the bleed air vents were relatively high. As a result, the interior cell density initially led to extremely low y^+ values, for which corrections were made to minimize artificial viscosity increases.

A grid sensitivity study was conducted with five meshes ranging between 450K – 2.5M cells. Across all angles of attack, the CFD solutions were found to show significant changes in the lift coefficient c_l until the cell count was approximately 1.7 M. However, the drag coefficient c_d showed little dependence on cell count below α = 7°. Ghoreyshi et al.[9] document the findings in greater detail.

C. Flow Regime and Simulation Parameters

CFD results were computed using both the commercially available code Cobalt[21] and the DoD-developed solver within the CREATE-AV/*Kestrel* software suite. Both codes are based on finite-volume methods and in addition to performing traditional RANS calculations, also have the capability to perform Delay-Detached Eddy Simulations (DDES).[22] For the 2-D simulations presented in this effort, the DDES functionality was not used. Cobalt simulations were run on the

Cray XE6 at the High Performance Computing and Modernization Program's (HPCMP) Engineering Research Development Center. Kestrel was used on the SGI ICE X System located at the AFRL DSRC.

The numerical method used by Cobalt is based on Godunov's first-order accurate, cell-centered, finite volume, exact Riemann solution method applicable to arbitrary cell topologies[23]. The spatial operator uses the exact Riemann Solver of Gottlieb and Groth, least squares gradient calculations using QR factorization to provide second order accuracy in space, and TVD flux limiters to limit extremes at cell faces[24]. A point implicit method using analytic first-order inviscid and viscous Jacobians is used for advancement of the discretized system. For time-accurate computations, a second order accurate Newton sub-iteration scheme is employed. Parallel performance is achieved using the ParMETIS domain decomposition library for optimal load balancing with a minimal surface interface between zones[25]. The code uses Message Passing Interface (MPI) for communication between processors, with parallel efficiencies above 95% on as many as 1024 processors and scales linearly up to 4000 processors.

The flow solver component of Kestrel[26] (kCFD) solves the unsteady, three-dimensional, compressible Navier-Stokes equations on hybrid unstructured grids. Its foundation is based on Godunov's first-order accurate, exact Riemann solver. Second-order spatial accuracy is obtained through a least squares reconstruction. The code also uses an implicit Newton sub-iteration method to improve time accuracy as well. Kestrel receives an eXtensible Markup Language (XML) input file generated by Kestrel User Interface and stores the solution convergence and volume results in a common data structure for later use by the Output Manager component. Some available turbulence models are the Spalart-Allmaras model, SARC, and DDES with SARC.

Table 1 documents the parameters and conditions used for the unsteady, 2nd order in time, simulations which resulted in a Reynolds number, $Re = 1.4 \times 10^6$ with a non-dimensional time step $\Delta t^* = 0.00868$.

Table 1. General Job File Inputs and "Test" Matrix

Parameter or Property	Value or Condition
Gas Model	Ideal Gas
Turbulence Model	SA
Newton Subiterations	3
Initial CFL	100
Iterations	30,000
Mach	0.01
α (deg)	0, 4, 8.5
Static Pressure (Pa)	64,091.088496
Static Temperature (K)	300
Time step (s)	0.00025
Velocity (m/s)	34.718871

Given these values, Figure 4 shows typical convergence histories for the lift coefficient. In particular, Figure 4 b, exhibits the unsteady nature associated with these configurations and flows. It has been the authors' experience that the unsteadiness of these flows requires well-documented and careful application of numerical methods in order to address differences seen in simulation results, especially as multiple, realistic looking, flow fields can produce similar integrated results. Indeed, the requirement for a ram-air validation program among the computational, experimental, and flight/drop test domains is strongly reinforced in this effort.

While both Cobalt and CREATE-AV/*Kestrel* were used for the initial testing of the baseline geometry with no bleed-air vents, the majority of the results in this work are for kCFD solutions. Figure 5 provides comparison data between the two codes for geometries with no BA vents and varying tail deflections. For $\alpha = 0°$ and 8.5° the two solvers produce similar results. However, for the $\alpha = 4°$ simulations, nontrivial differences were seen. These may have been due to different damping coefficients used within the codes. It was generally noted that both codes showed relatively large oscillations depending on angle of attack, tail deflection, and BA vent actuation. In light of the 2D nature of the simulations, limited validation data, and the relatively narrow angle of attack range associated with ram-air parachute flow fields, it was decided to focus the study at $\alpha = 8.5°$.

III. Simulation Results and Discussion

The figure of merit used throughout this discussion will be the lift-to-drag ratio, *L/D*. The primary purpose of this investigation is to investigate the effectiveness of different combinations of geometry configurations using BA vents and tail deflection for lateral and longitudinal control. *L/D* and turn rates are the primary figures of merit used during test drops of autonomously guided airdrop systems, and though the specific control effects of the control actuator combinations cannot be determined with 2D simulations, the numerical study will provide qualitative data as well as expand the capability to efficiently and effectively model the aerodynamic characteristics of ram-air canopies. *L/D* values reported represent averages over the last 10,000 iterations, and as such are denoted as L/D_{TA}. Each of the flow field snapshots was taken on the last iteration.

The 2D geometry also facilitates the development of a moving control surface simulation capability for future work to determine not only static aerodynamic forces and moments but also rates. In light of this long term goal, considering all combinations of control actuators was beyond the qualitative scope of this effort. Similarly, moment coefficients are not reported at this time.

Simulations results below were completed using 1024 processors. Each CPU had 2 GB of memory. Average total wall clock time per simulation was 3 hours.

The outline of this section will follow successively more complicated airfoil configurations/designs used and proposed for airdrop systems. The first section documents the simulation results of an airfoil shape which has been drop tested for several years. The following section gives the first results known to the authors of a high-fidelity simulation of a ram-air parachute with a deflected trailing edge. Section C details the flow field changes associated with various locations and orientations of a single bleed air vent. The final section addresses preliminary work associated with investigations of the combined effects of multiple bleed air vents and trailing edge deflections.

A. Ram-air Airfoil Section versus α—No TE Deflection

The results presented in Figure 6 provide a baseline flow reference for all other simulation results. These flows correlate well with the Cobalt simulation solutions presented in Figure 13 of Ghoreyshi et al.[9] At $\alpha = 0°$, a relatively strong eddy forms along the lower surface at the leading edge of the inlet. The eddy results from a combination of a flow across the "curled" sharp-edge[6] and the freestream flow reversal within the ram-air "cavity." As the angle of attack increases to

4°, this eddy loses energy. In combination with the reduced pressure along the upper surface, the reduction of the downward suction leads to a 250% increase in the L/D_{TA}. However, further increases in the angle of attack to 8.5° results in the L/D_{TA} decreasing to 8.0. The lower surface leading edge eddy has become smaller, but the flow over the upper surface has separated. It should be noted that parachutes rigged at $\alpha = 8.5°$ do not show this strong separation, which indicates a more detailed numerical study is required for validation. Ghoreyshi et al.[9] initiated such a program with promising initial results.

B. Ram-air Airfoil Sections with Deflected Trailing Edge: 50% and 100%

The effects of deflecting the trailing edge are illustrated in Figure 7. As in the non-deflected angle of attack sweep, the intensity of the lower surface leading edge eddy diminishes with increased deflection, and the penetration of the freestream flow through the open inlet is reduced. The upper surface flow separates earlier moving from approximately 0.25c for the non-deflected tail to 0.1c for the 100% deflected case. L/D_{TA} evolution follows accordingly, with a nonlinear decrease from 8 to 3.

C. Upper Surface BA Vent Variations, 0% Trailing Edge Deflection

The use of BA vents has been proven to be useful control actuators, and early simulation efforts have characterized applications of a vent located near the quarter chord point of the upper surface. Different locations and orientation of a single actuator are shown in Figure 8. The associated flow fields exhibit very distinct characteristics.

1. 0.2c—Front vs Rear Attachment: Figures 8a and 8b

In both cases the freestream flow passes through the inlet with minimal flow reversal. As such the spatial extent of the lower surface leading edge vortex is reduced. While still present for the front flap vent orientation, the eddy essentially disappears in the rear flap orientation.

The front flap vent flow forms a recirculation region in the interior "nose" of the canopy. Smaller regions of recirculation are seen in the regions aft of the vent location. At the vent a strong jet exits and combines with the accelerated flow from the front portion of the airfoil, and creates a virtual "spoiler" resulting in a separation region larger than seen in Figure 6c. Compared to the baseline geometry, the L/D_{TA} was reduced from 8.0 to 1.2.

Using the rear flap vent, however, the L/D_{TA} increased substantially to 59.1. This configuration functions as a leading edge slat on traditional rigid wings. A.M.O. Smith[27] provides a detailed analysis of such flows. As applied in this simulation, the freestream flow enters the inlet unimpeded and upon exiting the vent interacts with the wake of the leading element to produce a synergistic lift effect. Several parachute manufacturers implemented a version of this concept in the 1980s as a fixed configuration located much further forward than the 0.2c location. However, the use in an active control paradigm was not investigated. Section D below includes an illustration of extending the multi-element airfoil configuration. If used in combination with trailing edge deflection, it is envisioned that ram-air parachute systems would allow for an increased angle of attack range and permit greater control of kinetic energy during the landing phase.

Interestingly, both Gavrilovski et al.[4], using small-scale ($2.7m^2$) paragliding-style canopy, and Bergeron et al.[5], using airdropped systems, saw small increases in the *L/D* when the front flap vent was activated between 20% and 40% of full scale deflection. However, for the rear flap case, neither reported an *L/D* increase of the magnitude seen in these 2D simulations. Of final note, simulations have also been conducted with a concave rear flap, intended to increase the vertical momentum transfer during vent operation, but results are inconclusive at this time.

2. Front Flap—0.2c vs 0.6c

To investigate the value of an array of bleed air vents as well as collect data for control effectiveness, simulations were conducted with a front flap bleed air vent located at 0.6c. In this geometry, the freestream flow field experiences a much greater pressure, relative to the 0.2c case, upon entering the inlet. Effectively the rear flap vent has created a shorter cavity flow with an associated increased flow reversal at the inlet. This reversed flow contribution leads to an increase in the lower surface leading edge eddy vorticity. The L/D_{TA} is twice the value of the 0.2c front flap vent, for the same deflection. Therefore, this actuation location may be useful for higher fidelity control of the system *L/D*.

D. Coupled Actuator Influences

1. BA Vent Coupled with TE Deflection

Figure 9 illustrates several combinations of BA vents with a TE deflection. In combination with Figure 8a., Figures 9a., and 9b. show the dependence of the 0.2c front flap vent geometry as the trailing edge is deflected from 0% to 50% to 100%. The corresponding L/D_{TA} values are 1.2, 2.1, and 1.8. The apparent nonlinear nature of the L/D_{TA} would possibly make control law development and application more difficult, and therefore merits further analysis. Though Figure 9a. shows a reattachment of the flow, this is an artifact of the last iteration snapshot of a time dependent flow. The time dependence is also evident upon closer inspection of the flow along the lower surface leading edge. In Figures 9a. and 9b. two and three small eddies, respectively, are seen shedding. The spatial extent of these lower surface eddies also appear to be smaller than in the non-BA vent cases. This behavior corresponds to the reduced flow reversal seen with the opened vent.

Figure 9c. also follows the behavior seen in the previous simulations, as the positioning of the front flap vent at 0.6c again allows a greater portion of the freestream flow to enter the cavity. The greatest portion of the flow reversal does not occur until the flow has reached the front flap vent. Comparing Figures 8c. and 9c. with the other simulated flows, one also notices a decrease in the pressure fields downstream of the vent. As the control forces required to move the trailing edge are an order of magnitude greater than the forces required to move the bleed air vents[5], the pressure relief provided by the 0.6c vent may allow for a more efficient trailing edge actuator.

2. Multiple Upper Surface Bleed Air Vent

The last set of simulations, Figure 10, show coupling phenomena which are also being investigated separately in the NSRDEC Precision Airdrop Enhancements test program. Figure 10a. is noteworthy from the previous discussion and understanding of multi-element airfoils. As has been shown for traditional rigid wing airfoils, two elements are better than one, and in Smith's words[27], "if properly designed—the more slots, the better." However, in this application, the middle element, the portion of the upper surface between the 0.2c and 0.6c rear flap vents, experiences a negative contribution from the downstream trailing edge element due to the reduced flow interior to the cavity after the 0.2c vent.

The configuration shown in Figure 10b. introduces much more promise from a control authority perspective. In the rear portion of the interior of the airfoil section, after the 0.6c front vent, the reduced pressure could serve to reduce the forces needed for trailing edge deflection. Then, a combination of a third modality, two bleed air vents and trailing edge deflection, could provide needed capability for an autonomously guided airdrop system.

IV. Conclusion

Unsteady computational simulation results have been presented for a number of different combinations of 2D ram-air airfoil sections, based on a reference section used for airdrop cargo delivery. The tools and standards of practice developed for this study serve as a baseline for 3D computational fluid dynamics and fluid-structure interaction research. Criteria from a parallel study by Ghoreyshi et al.[9] were followed. The tested geometries included empirically defined trailing edge deflections. In addition, several new bleed air vent configurations were tested. The L/D_{TA} ranged between 1.2 and 59.1, and for the appropriate cases, qualitatively correlated with results from airdrop tests. Distinct flow fields were observed with each airfoil section, including the development of an eddy at the leading edge of the lower surface. The lower surface eddy was, in general, found to be much smaller than reported in several other studies. The eddy characteristics varied with angle of attack, trailing edge deflection, and bleed air vent actuation.

The most significant conclusion resulting from this and the Ghoreyshi et al. studies is the critical need for an aerodynamic database for validation. This requirement was also recognized by Potvin et al.[28] for the much larger Aerodynamic Decelerator Systems community. However, the current work proposes a focused program on rigid models in order to jump start the validation effort. Future work would then expand the control actuator parameter sweep and include fluid-structure interactions.

Acknowledgements

The authors would like to first acknowledge the support of the Natick Soldier Research Development and Engineering Center Airdrop Technology Team and the DoD HPCMP. In particular, the HPCMPs Computational Research and Engineering Acquisition Tools and Environments—Air Vehicles (CREATE-AV) team has provided substantial resources and help, including valuable meshing inputs from many members participating in the program's Pilot Projects. Finally, Mehdi Ghoreyshi and Jürgen Seidel extend their appreciation for the researchers and technicians at the Aeronautics Research Center and the High Performance Computing Research Center at the USAF Academy who have time and again provided critical assistance and insights.

This material is based in part on research sponsored by the US Air Force Academy under agreement number FA7000-10-2-0026. The U.S. Government is authorized to reproduce and distribute reprints for Governmental purposes notwithstanding any copyright notation thereon. The views and conclusions contained herein are those of the authors and should not be interpreted as necessarily representing the official policies or endorsements, either expressed or implied, of the US Air Force Academy or the U.S. Government.

References

[1] Bergeron, H., Private communication.

[2] Eiff, J. and Hayhurst, J., "Classic Accuracy Manual," Eiff Aerodynamics, 1996.

[3] Higgins, M. W., "Control System for Ram Air Gliding Parachute," U.S. Patent 4,175,722, Nov 1979.

[4] Gavrilovski, A., Ward, M., and Costello, M., "Parafoil Control Authority with Upper-Surface Canopy Spoilers," Journal of Aircraft, 2012, Vol. 49: 1391-1397.

[5] Bergeron, K., Ward, M., and, M, and Costello, M, "Aerodynamic Effects of Parafoil Upper Surface Bleed Air Actuation," AIAA-2012-4737.

[6] Ward, M. and Costello, M, "AG100 Spoiler Flight Test Results," Contract Report, Contract Number: W9124R-09-P-1088,16 August 2011.

[7] Bergeron, K., Ward., M., Costello, M., and Tavan, S., "AG100 and Bleed-Air Actuator Airdrop Testing," 22nd ADS Conference, Daytona Beach, FL, 2013.

[8] Ward, M., "Adaptive Glide Slope Control for Parafoil and Payload Aircraft," PhD thesis, Georgia Institute of Technology, 2012.

[9] Ghoreyshi, M., Seidel, J., Bergeron, K., Jirasek, A., Lofthouse, A.J., and Cummings, R. M.,"Predicition of Aerodynamic Characteristics of a Ram-Air Parachute," presented at AIAA Aviation 2014 Conference and Exposition, 16-20 June 2014.

[10] Fogell, N., "Fluid-structure interaction simulations of the inflated shape of ram-air parachutes, PhD thesis, Imperial College London, 2014.

[11] Mittal, S., Saxena, P., and Singh, A., "Computation of two-dimensional flows past ram-air parachutes," Int. J. Numer. Meth. Fluids 2001: 35: 643-667.

[12] Balaji, R., Mittal, S., and Rai, A. K., "Effect of leading edge cut on the aerodynamics of ram-air parachutes," International Journal for Numerical Methods in Fluids, 47(1):1{17, 2005.

[13] Mohammadi, M. and Johari, H., "Computation of Flow over a High-Performance Parafoil Canopy," 2010, Journal of Aircraft, 0021-8669 vol.47 no.4 (1338-1345).

[14] Boffetta, G., and Ecke, R. E., "Two-Dimensional Turbulence," Ann Rev Flu Mech, 2012 44: 427-51.

[15] Hiraki, K and Hidaka, Y, "Aerodynamic Characteristics of Compulsively-Inflated Paraglider for Mars Exploration," AIAA 2013-1305.

[16] Ware, G.M., and Hassell, J. L., "Wind-Tunnel Investigation of Ram-Air-Inflated All-Flexible Wings of Aspect Ratios 1.0 to 3.0," Technical Report, NASA, 1969, TM SX-1923.

[17] Cummings, R.M., Morton, S.A., and McDaniel, D.R., "Experiences in Accurately Predicting Time-Dependent Flows," Progress in Aerospace Sciences, Vol. 44, No. 4, 2008, pp. 241-257.

[18] Lee, C. and Li, P, "geometri Properties of Parachutes Using 3-D Laser Scanning," J. of Aircraft Vol 44, No. 2, March April 2007, 377-385.

[19] Matos, C., Mahalingham, R., Ottinger, G., Klapper, J., Funk, R., and Komerath, N, "Wind Tunnel Measurements of Parafoil Geometry and Aerodynamics," AIAA 98-0606.

[20] Bergeron, K., Fejzi, A, and Tavan, S., "AccuGlide 100: Precision Airdrop Guidance and Control via Glide Slope Control," AIAA 2011-2530.

[21] "Cobalt," Cobalt Solutions [website], http://www.cobaltcfd.com/ [retrieved 23 May 2014].

[22] Strang, W., Tomaro, R., and Grismer, M., "The Defining Methods of Cobalt60: A Parallel, Implicit, Unstructured Euler/Navier-Stokes Flow Solver," *AIAA Paper 1999-0786*, 1999.

[23] Godunov, S. K., "A Finite Difference Method for the Computation of Discontinuous Solutions of the Equations of Fluid Dynamics", *Mat. Sb.*, 47:357-393, 1959.
[24] Gottlieb, J. J. and Groth, C. P. T. (1988). "Assessment of Riemann solvers for unsteady one-dimensional inviscid flows for perfect gases." *J. Comp. Phys.*, 78(2):437–458.
[25] Karypis, G., Schloegel, K, Kumar, V. (1997). ParMETIS: Parallel Graph Partitioning and Sparse Matrix Ordering Library Version 1.0.
[26] Morton, S.A., McDaniel, D.R., Sears, D.R., Tillman, B., and Tuckey, T.R., "Kestrel: A Fixed Wing Virtual Aircraft Product of the CREATE Program," AIAA 2009-0338.
[27] Smith, A.M.O., "High-Lift Aerodynamics," 1975, Journal of Aircraft,Vol 12, No 6, (501-531).
[28] Potvin, J., Bergeron, K., Brown, G., Charles, R., Desabrais, K., Johari, H., Kumar, V., McQuilling, M., Morris., A., Noetscher, G., Tutt, B., "The Road Ahead: A White Paper on the Development, Testing and Use of Advanced Numerical Modeling for Aerodynamic Decelerator Systems Design and Analysis", AIAA 2011-2501.

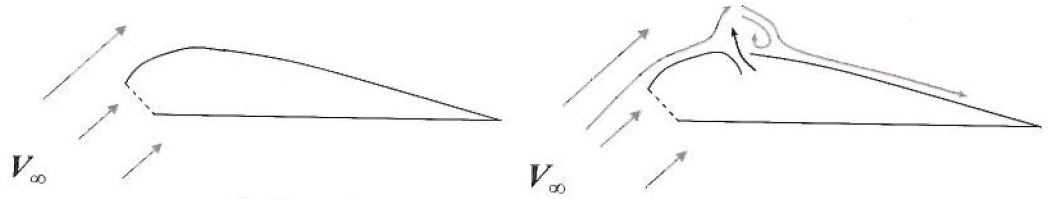

a) Closed **b) Open**

Figure 1. Notional depiction of parafoil aerodynamics with upper surface bleed air spoiler[5]

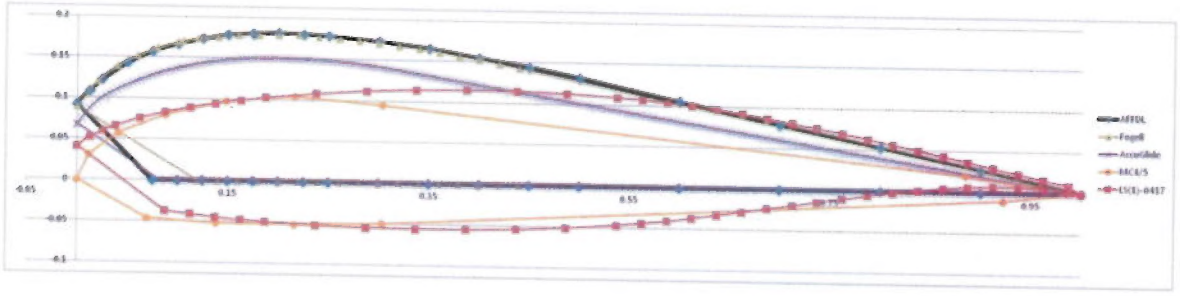

Figure 2. Ram-air airfoil sections

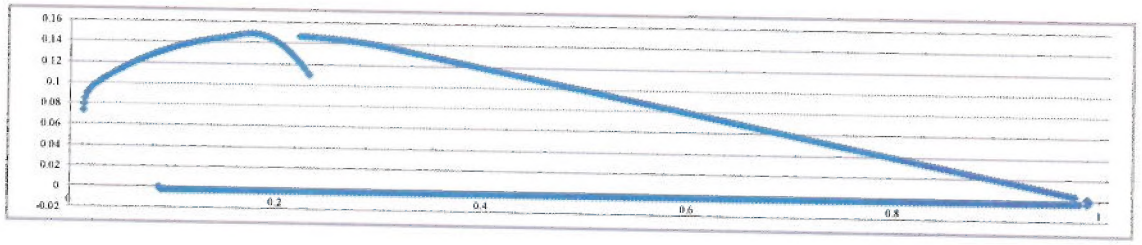

Figure 3. Baseline Geometry with bleed air vent located at $0.2c^5$

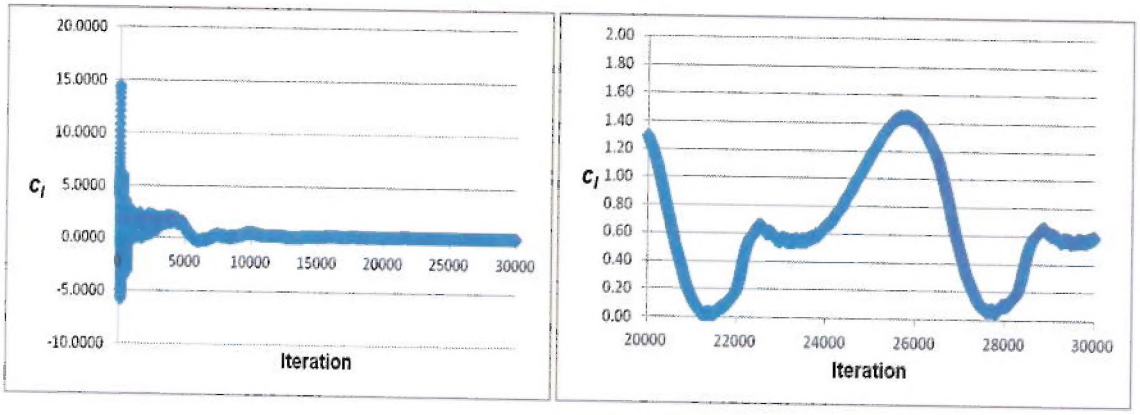

a. 0% Tail Deflection b. 50% Tail Deflection

Figure 4. Convergence Plots, C_l : $\alpha = 8.5$, 0.2c BA Vent

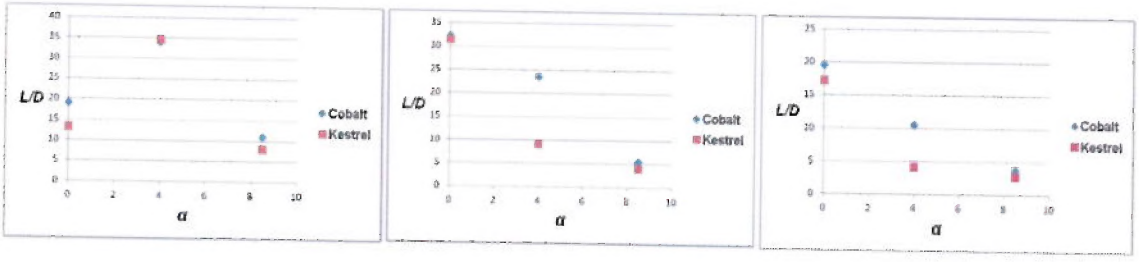

a. 0% b. 50% c. 100%

Figure 5. Cobalt vs Kestrel—Trailing Edge (TE) Deflection

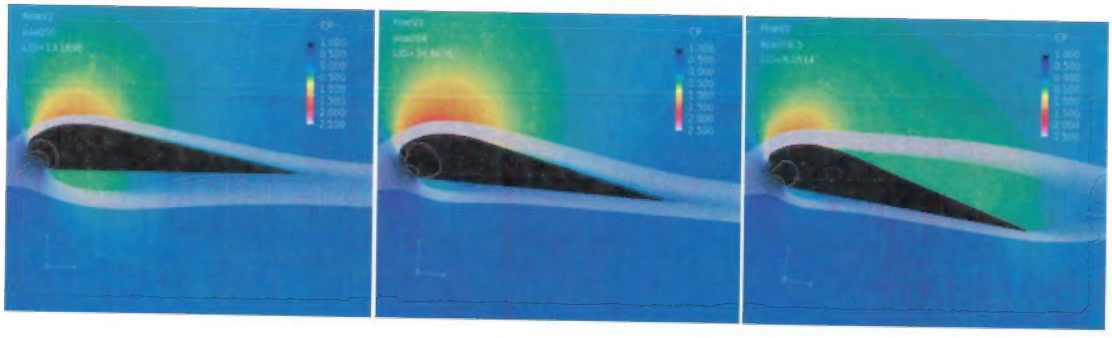

a. 0° b. 4° c. 8.5°

Figure 6: Ram-air Airfoil Section versus α, angle of attack

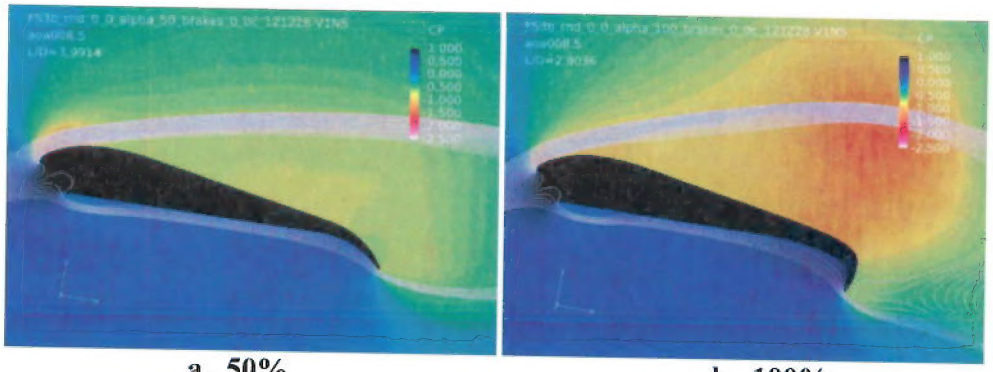

a. 50% b. 100%

Figure 7: Ram-air Airfoil Sections with TE Deflection

a. 0.2c-front flap b. 0.2c-rear flap c. 0.6c-front flap

Figure 8: Upper Surface BA Vent Variations, 0% TE Deflection

a. 0.2c-front flap, 50% b. 0.2c-front flap, 100% c. 0.6c-rear flap, 100%

Figure 9: BA Vent Coupled with TE Deflection

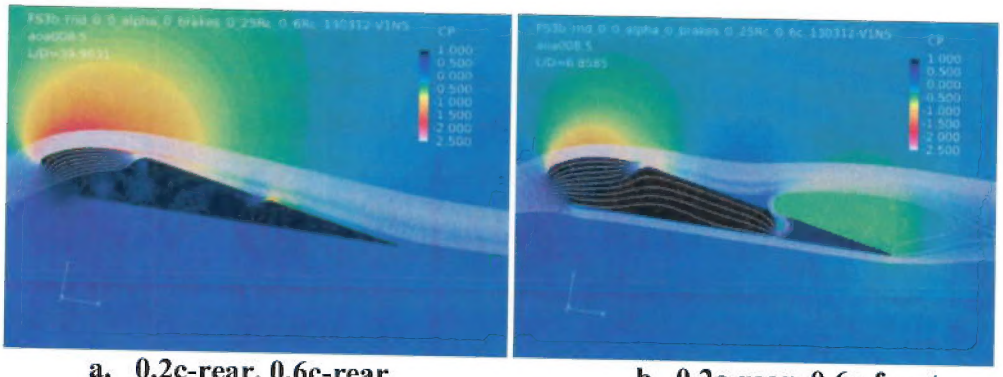

a. 0.2c-rear, 0.6c-rear b. 0.2c-rear, 0.6c-front

Figure 10: Multiple Upper Surface Bleed Air Vents